Hindawi
Wireless Communications and Mobile Computing
Volume 2021, Article ID 6408772, 12 pages
https://doi.org/10.1155/2021/6408772

Research Article

Optimization of Historic Building Survey Technology under Artificial Intelligence Wireless Network Technology Environment

Wei Tan,[1,2] **Ye Fen**,[2] **and Qi Yuan**[3]

[1]*School of Architecture and Planning, Hunan University, Changsha 410082, Hunan, China*
[2]*College of Landscape Architecture, Central South University of Forestry and Technology, Changsha, 410004 Hunan, China*
[3]*Branch of Landscape and Light Environment Design, Hunan University Design and Research Institute Co., Ltd., Changsha, 410006 Hunan, China*

Correspondence should be addressed to Wei Tan; vicotrtan@hnu.edu.cn

Received 28 October 2021; Revised 25 November 2021; Accepted 27 November 2021; Published 16 December 2021

Academic Editor: Vinoth Babu Kumaravelu

Copyright © 2021 Wei Tan et al. This is an open access article distributed under the Creative Commons Attribution License, which permits unrestricted use, distribution, and reproduction in any medium, provided the original work is properly cited.

In order to optimize the technology of the building, the damage identification of the building structure is studied. Firstly, back propagation neural network (BPNN) and information fusion technology are used to build neural network models. Secondly, the established model is trained. Finally, the displacement mode, natural frequency, Modal Assurance Criterion (MAC), and three kinds of information fusion with only one characteristic information are used as input data to analyse the results of BPNN identification damage. The results show that when the natural frequency is used as the sensitive feature of damage, the accuracy is the highest. The difference between the network output value and the expected value is the smallest, the network output is the most stable, and the network recognition effect is the best. The network output of a mixture of two damage depths is compared with the output of a single damage depth. The data of the network training set composed of the feature data with damage depth of 20 mm and 5 mm has higher accuracy and more accurate damage recognition. This research provides a reference for the optimization of building survey technology and has certain practical value.

1. Introduction

Historical architecture is a treasure produced in the process of human history development. It has important historical value, scientific value, artistic value, social value, and economic value. Therefore, the protection of historical buildings is urgent. At present, there are many new and old buildings in various countries in the world, and the service life of these buildings will decrease over time. Since the 1950s, the world population has grown exponentially, the economy is developing rapidly, and human beings exploit large amounts of natural resources. These have led to frequent environmental and geological disasters all over the world. China has experienced several major earthquake disasters. Ground fissure is a kind of superficial geological disaster phenomenon; its occurrence frequency and disaster scale show an increasingly serious trend. As of 2019, according to incomplete statistics of more than 200 cities and counties in the seven provinces of Shaanxi, Shanxi, Shandong, Jiangsu, Hebei, Henan, and Anhui, there are more than 1,000 ground fissures in total. These ground fissures have caused serious damage to various building structures, transportation facilities, urban lifeline projects, and land resources. Over the years, the direct and indirect economic losses caused by ground fissure disasters amounted to hundreds of millions of yuan. Building damage will bring some safety issues. Ground fissures can cause wall cracks, foundation collapse, and even collapse of buildings. Therefore, the occurrence of building cracks is inevitable [1]. Due to the continuous development of secondary hidden cracks, some ancient buildings gradually appeared cracks and suffered varying degrees of damage [2]. Therefore, long-term monitoring of the health status of existing building structures and covering them in different areas of ground fissure activity provide the possibility for traditional buildings to cross ground fissures [3].

Ground fissures can cause a series of hazards such as cracking of the walls of the building structure, damage to

the load-bearing components, settlement, and collapse of the foundation. These hazards not only affect the normal use of buildings but also cause underground pipelines to rupture and road dislocations. The ground fissure has caused irreversible damage to human production and life. The contradiction between large-scale urban construction and ground fissure disasters has become increasingly prominent. Nowadays, with the continuous development of science and technology, the emergence of artificial intelligence (AI) and network technology, the intelligent diagnosis, and detection technology of building structures have a wide range of application prospects [4]. Various survey techniques are widely used in construction, water conservancy, and other engineering fields [5]. The structural health monitoring system uses remote sensing technology to analyse the static and dynamic characteristics of the structure and monitor changes. A structural health monitoring system is established at the appropriate location. By detecting the real-time response of the structure in different states, the force state of the structure is obtained. In this way, it can be judged whether the structure is damaged. The current health status of the building structure is obtained [6–8].

For buildings with different structures, a single-information judgment criterion cannot accurately identify structural damage, nor can it improve the reliability of structural safety evaluation. Information fusion technology can realize the processing and fusion of multisource sensor data, extract key features, and comprehensively evaluate the safety performance of the structure. Compared with the technology that only considers a single damage feature, the information fusion technology can greatly improve the sensitivity of the structural health monitoring system to damage. Information fusion technology can reduce the impact of uncertain factors on damage identification and improve the robustness of the health monitoring system. Meanwhile, the combination of artificial neural network (ANN) and information fusion is applied to structural damage identification. This is conducive to the visual development of structural health monitoring. Therefore, the BPNN model is used to study structural damage identification and location based on modal frequency, displacement mode, and modal confidence criteria. The information fusion of the three types of feature information is used in damage identification and location. The recognition result of the information fusion and the recognition result of a single feature are compared and analysed. The combination of information fusion and ANN is used in structural damage identification. This has far-reaching practical significance for the monitoring of structural safety performance.

2. Literature Review

As a part of machine learning, the most basic way to realize deep learning is to use the characteristics of neural networks to use the network structure of multiple hidden layers to extract data features. This method does not require human intervention and includes models such as autoencoders, convolutional neural networks, and deep confidence networks. With the advent of the big data process and the rapid improvement of computer hardware performance, the recognition method of deep learning has become the research object of many researchers. Yu et al. (2019) [9] proposed a building structure damage recognition and location method by deep convolutional neural network (DCNN), which showed that this method had good generalization ability and high recognition accuracy. Liu et al. (2019) [10] proposed a method by parameter sensitivity to identify structural damage and damping defects of nonclassical damping shear buildings. Wang et al. (2021) [11] proposed a new method for structural damage identification by the low accuracy of structural damage recognition by time series data, combined with the advantages of Hilbert-Huang Transform and deep neural networks. Gao and Mosalam (2018) [12] implemented the most advanced deep learning technology in the application of civil engineering, that is, identifying structural damage from images. Inspired by the challenges of ImageNet and the development of computer hardware, they proposed the concept of structured ImageNet. Among them, four original baseline identification tasks are included: component type identification, peeling state inspection, damage level evaluation, and damage type determination. They select relatively few images from Structural ImageNet and manually label them according to four recognition tasks. In order to avoid overfitting, the transfer learning of Visual Geometry Group (VGGNet) was introduced, and two different strategies were adopted. This method is feature extraction and fine-tuning. According to the characteristics of these two strategies, two experiments were designed to find relatively optimal model parameters and applicable scope. The models obtained by these two strategies show good recognition results and different application potentials. Among them, feature extraction and fine-tuning can be used for preliminary analysis and further improvement, respectively. These results indicate the potential application of deep transfer learning in image-based structural damage recognition. The structural damage recognition system is an important part of the structural health monitoring system. The combination of ANN and damage recognition has become a research hotspot.

Neural networks belong to intelligent recognition, and there are some problems in practical applications. Neural networks need a large amount of sample data to train, and the training time is long. Meanwhile, the neural network may fall into a local minimum during the training process. More importantly, the recognition results of neural network methods are very dependent on the selection and construction of damage indicators. How to choose and construct damage-sensitive indicators is a problem that needs to be solved urgently.

3. Materials and Methods

3.1. Structural Damage Recognition. There are certain requirements for structural damage identification indicators. Damage must meet certain conditions before it can be used for identification. The specific conditions are shown in Figure 1.

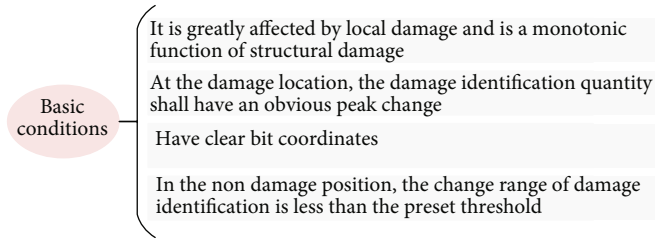

Figure 1: Necessary conditions for damage identification indicators.

(1) When an object vibrates freely, its displacement varies with time according to sine or sine curve. The frequency of vibration has nothing to do with the initial conditions and is related to the inherent characteristics of the system (such as mass, shape, and material), known as the natural frequency. The corresponding period is called inherent period. In the engineering structure, the parameters of the natural frequency are easy to obtain and have high accuracy [13]. The characteristic equation about the natural vibration of the system can be expressed as

$$(K - \lambda_i M)\phi_i = 0. \tag{1}$$

K is the stiffness matrix of the structure, M is the mass matrix, ϕ_i is the natural mode shape, and ${\phi_i}^T M\phi_i = 1$.

Suppose the number of the structural unit is r, and the total number of units is m. The stiffness is matrixed by Equation (1), which is expressed as

$$K = \sum_{r=1}^{m} p_r K_r^e. \tag{2}$$

K_r^e is the element stiffness matrix, and p_r is the quality of the structure. When $p_r = 1$, the structure is not damaged. When $p_r = 0$, the damage of this structure is very serious, and it has been destroyed. Under normal circumstances, if the structure is damaged, its stiffness matrix will produce certain variables for frequency and mode shape. Therefore, the perturbation equation of the structural equation can be expressed as

$$\{(K + \Delta K) - (\lambda_i + \Delta\lambda_i)(M + \Delta M)\}(\phi_i + \Delta\phi_i) = 0. \tag{3}$$

ΔK represents the change in the stiffness matrix when the structure is damaged, ΔM represents the change in the mass matrix when the structure is damaged, $\Delta\lambda_i$ is the change in the eigenvalue, and $\Delta\phi_i$ is the change in the eigenvector. Equation (3) can be expanded, as shown in

$$\Delta K\phi_i - \Delta\lambda_i M\phi_i = \lambda_i M\Delta\phi_i - K\Delta\phi_i. \tag{4}$$

Both K and M are real number matrices. Multiply the left side of Equation (4) by ϕ_i^T, as shown in

$$\Delta\lambda_i = \frac{\phi_i^T \Delta K\phi_i}{\phi_i^T M\phi_i}. \tag{5}$$

When the structure is damaged, the stiffness will decrease, and there will be $\Delta K \le 0$, so $\Delta\lambda_i \le 0$. Equation (6) can be obtained from Equation (2):

$$\Delta K = -\sum_{r=1}^{m}(1 - p_r)K_r^e = \sum_{r=1}^{m}\alpha_r K_r^e. \tag{6}$$

K_r^e is the element stiffness matrix, p_r is the quality of the structure, and α_r and p_r are corresponding, referring to the quality of the structure. Substitute Equation (6) into Equation (5), for single damage structure, as shown in

$$\Delta\lambda_i = -\frac{\alpha_r \phi_i^T K_r^e \phi_i}{\phi_i^T M\phi_i}(i = 1, 2, \cdots, n). \tag{7}$$

n is the degree of freedom. Equation (7) shows that the frequency change of the structure is affected by two factors, the degree of damage α_r and the location of the damage.

(2) Damage identification by strain or displacement mode, the expressions of structural displacement and strain are shown in Equations (8) and (9)

$$v(x) = \sum_{r=1}^{\infty}\varphi_r(x)q_r(t), \tag{8}$$

$$\varepsilon(x) = \sum_{r=1}^{\infty} \phi_r(x) q_r'(t). \tag{9}$$

φ_r and ϕ_r are the rth order displacement mode and strain mode of the structure; $q_r(t)$ and $q_r'(t)$ are the displacement mode and strain mode coordinates, respectively. Suppose u, v, and w are the displacements of the elastic body corresponding to the x, y, and z axes, respectively, and the displacement can be expressed as Equation (10) through modal superposition:

$$u = \sum_{r=1}^{m} q_r \phi_r(x). \tag{10}$$

If the strain mode is set to ψ_r^{ε}, then ψ_r^{ε} can be expressed as shown in

$$\psi_r^{\varepsilon} = \frac{\partial}{\partial x} \phi_r(x). \tag{11}$$

Taking the derivative of Equation (10), the strain ε_x of the structure can be obtained as

$$\varepsilon_x = \frac{\partial u}{\partial x} = \frac{\partial}{\partial x} \sum_{r=1}^{m} q_r \phi_r(x) = \sum_{r=1}^{m} q_r \frac{\partial \phi_r(x)}{\partial x} = \sum_{r=1}^{m} q_r \psi_r^{\varepsilon}(x). \tag{12}$$

Assuming that the displacement is expressed in the form of a vector, then the displacement vector $\{x\}$ and the displacement mode are as

$$\{x\} = \{u \quad v \quad w\}, \tag{13}$$

$$\{\varphi_r\} = [\{\varphi_r^u\} \quad \{\varphi_r^v\} \quad \{\varphi_r^w\}]. \tag{14}$$

The displacement response can be obtained by superimposing the displacement mode, which is expressed in

$$\begin{Bmatrix} \{u\} \\ \{v\} \\ \{w\} \end{Bmatrix} = \sum_{r=1}^{m} q_r \begin{Bmatrix} \{\varphi_r^u\} \\ \{\varphi_{ry}^v\} \\ \{\varphi_{rz}^w\} \end{Bmatrix}. \tag{15}$$

Suppose the normal strain in the three-dimensional space is ε_x, ε_y, and ε_z. According to the theory of elasticity, the displacement, strain, and shear strain can be expressed in the form of a matrix, as shown in

$$\begin{bmatrix} \varepsilon_x & \alpha_{yx} & \alpha_{zx} \\ \alpha_{xy} & \varepsilon_y & \alpha_{zy} \\ \alpha_{xz} & \alpha_{yz} & \varepsilon_z \end{bmatrix} = \begin{bmatrix} \frac{\partial u}{\partial x} & \frac{\partial v}{\partial x} & \frac{\partial w}{\partial x} \\ \frac{\partial u}{\partial y} & \frac{\partial v}{\partial y} & \frac{\partial w}{\partial y} \\ \frac{\partial u}{\partial z} & \frac{\partial v}{\partial z} & \frac{\partial w}{\partial z} \end{bmatrix}, \tag{16}$$

$$\begin{aligned} \gamma_{xy} &= \alpha_{yx} + \alpha_{xy}, \\ \gamma_{yz} &= \alpha_{yz} + \alpha_{zy}, \\ \gamma_{xz} &= \alpha_{xz} + \alpha_{zx}. \end{aligned} \tag{17}$$

Normally, the normal strain is measured in the actual measurement. If only the normal strain is considered, then the corresponding strain tensor can be expressed as

$$\begin{bmatrix} \varepsilon_x \\ \varepsilon_y \\ \varepsilon_z \end{bmatrix} = \sum_{r=1}^{m} q_r \begin{bmatrix} \frac{\partial}{\partial x}\{\varphi_r^u\} \\ \frac{\partial}{\partial y}\{\varphi_r^v\} \\ \frac{\partial}{\partial z}\{\varphi_r^w\} \end{bmatrix} = \sum_{r=1}^{m} q_r \begin{bmatrix} \{\psi_r^{\varepsilon}\}x \\ \{\psi_r^{\varepsilon}\}y \\ \{\psi_r^{\varepsilon}\}z \end{bmatrix}. \tag{18}$$

$\{\psi_r^{\varepsilon}\}$ is the mode shape of the rth strain mode. In actual measurement, the strain mode shape corresponding to the measured strain can be expressed as

$$H_{ij}^{s} = \sum_{r=1}^{m} \frac{\psi_{ir}^{s} \phi_{jr} / k_r}{1 - ((\omega^2/\omega_r^2) + 2j\xi_r(\omega/\omega_r))}. \tag{19}$$

Among them, ξ is the damping ratio, and ω is the circular frequency of the structure. The specific calculation equations for these two quantities are

$$\xi_r = \frac{c_r}{2\sqrt{m_r k_r}}, \tag{20}$$

$$\omega_r = \sqrt{\frac{k_r}{m_r}}. \tag{21}$$

If the frequency of the Sth order is the same as the external excitation, Equation (19) can be changed to

$$H^{\varepsilon} = \frac{\psi_{ms}^{\varepsilon} \phi_{ms}}{2j\xi_s k_s} + \sum_{r=1, r\neq s}^{m} \frac{\psi_{ir}^{s} \phi_{jr} / k_r}{((\omega^2/\omega_r^2) + 2j\xi_r(\omega/\omega_r))}. \tag{22}$$

Except for the Sth order, the modes of other orders are not considered. Then, Equation (22) is simplified, as shown in

$$H_{ij}^{\varepsilon} = \frac{\varepsilon_i(\omega_s)}{F_m(\omega_s)} = \frac{\psi_{ms}^{\varepsilon} \phi_{ms}}{2j\xi_s k_s}. \tag{23}$$

The corresponding Sth order strain mode can be expressed as

$$\psi_{ms}^{\varepsilon} = \frac{2j\xi_s k_s}{\phi_{ms} F_m(\omega_s)} \varepsilon_i(\omega_s). \tag{24}$$

When the structure is damaged, the internal stress distribution will be affected. Its stress distribution will change, which will affect the strain mode. If $\{\psi_r^{\varepsilon}\}$ and $\{\psi_{rd}^{\varepsilon}\}$ are

the predamage and postdamage strain modes, respectively, the variation of the strain mode can be expressed as

$$\Delta\psi_r^{\varepsilon}(i) = \psi_{rd}^{\varepsilon}(i) - \psi_r^{\varepsilon}(i) m_r c_{rk}. \tag{25}$$

Under different working conditions, the damage of the structure is distinguished and located by the change of the strain mode.

(3) Damage identification by modal confidence criterion. If the structure is damaged, each corresponding mode shape will change. The mode shape is expressed by Modal Assurance Criterion (MAC) [14], as shown in

$$MAC(\phi) = \frac{\left(\phi_{fj}, \phi_{dj}^T\right)}{\left(\phi_{fj}, \phi_{fj}^T\right)\left(\phi_{dj}, \phi_{dj}^T\right)}. \tag{26}$$

ϕ_{fj} and ϕ_{dj} are the jth mode modes before and after damage, respectively. Equation (26) is the relationship between the mode shapes before and after damage.

3.2. Information Fusion Technology. In the early days, the information fusion technology was researched and applied because of its military needs. At that time, the information fusion technology was considered to start from multiple sensor data and related information sources, combined with the evaluation process, to achieve the positioning of the target and the comprehensive evaluation of the threat and importance of the battlefield. The basic principle of information fusion is by the biological brain processing a variety of information streams, combined with computer technology, the information acquisition system for regular processing [15–17]. Calculate, analyse, and preprocess to get the status information of the target. Combining different datasets, more structural information is gotten.

In the information fusion process, the detected information is converted into electrical signals, and then, the converted signals are converted into digital signals. After preprocessing and denoising, signal processing features are extracted from feature fusion or direct data fusion [18]. Its main advantage is multisensor information fusion technology can obtain data integration through multiple sets of sensors and can quickly and effectively process information [19]. If part of the information fails during the information processing, other information can be added, and the stability of the system can be improved.

According to the abstraction level of the data, the information fusion system can be classified (as shown in Table 1).

3.3. BPNN. BPNN is a back propagation algorithm added to the structure of the feedforward network. It has not only input and output nodes, but also one or more hidden layer nodes, which is a unidirectional propagation multilayer forward network [20, 21]. BPNN consists of three parts: input layer, hidden layer, and output layer. The hidden layer can have multiple layers, and each layer can contain a different number of neurons [22]. When BPNN works, import data samples through the input layer. Then, through a series of mathematical calculations, the law between the data is obtained [23]. Finally, use these laws to calculate all forecast datasets to get the forecast results. In the calculation process, the data propagates forward, and the weights and biases of hidden neurons are obtained randomly [24]. The neural network propagates forward to obtain the sum of each neuron and transmits the data on the neuron to the next layer of neurons through the activation function. The BPNN structure with 2 hidden layers is shown in Figure 2.

3.4. Establishment of Neural Network Algorithm. In the learning process of BPNN, errors are propagated back. The core of the BPNN algorithm is the weight adjustment process [25]. Take h-layer BPNN as an example to establish the BPNN algorithm:

(1) Parameter definition. Suppose the total number of samples is n, and the weight matrix is V_{ij}. Among them, $i = 1, 2, \cdots, n$; $j = 1, 2, \cdots, m_1$. The sample value of the input layer is expressed as

$$X = (x_1, x_2, \cdots, x_n). \tag{27}$$

Layer 1: there are m_1 neurons, and the weight matrix is W_{ij}^1, where $i = 1, 2, \cdots, m_1$; $j = 1, 2, \cdots, m_2$. The output value is

$$y_1 = \left(y_1^1, y_2^1, \cdots, y_{m_1}^1\right). \tag{28}$$

Layer 2: there are m_2 neurons, and the weight matrix is W_{ij}^2, where $i = 1, 2, \cdots, m_2$; $j = 1, 2, \cdots, m_3$. The output value is shown in

$$y_2 = \left(y_1^2, y_2^2, \cdots, y_{m_2}^2\right). \tag{29}$$

Layer h: set up m_k neurons, l output layer samples, and the weight matrix is expressed as W_{ij}^h, where $i = 1, 2, \cdots, m_k$; $j = 1, 2, \cdots, l$; then, the output value is as shown in

$$y_k = \left(y_1^k, y_2^k, \cdots, y_{m_k}^k\right). \tag{30}$$

The sample value of the output layer can be expressed as

$$O = (o_1, o_2, \cdots o_l). \tag{31}$$

(2) The process of feedforward. Initialize first, given the input sample, expected output and training sample data, the weight is arbitrarily selected on (-1, 1) [26]. The "gradient descent method" is used for learning. The weights of the neural network are

Table 1: Information fusion system classification.

Name	Specific meaning
Pixel-level fusion	The data collected by the system is directly used for information fusion. It can retain the original information as much as possible and provide a better decision for the system to identify identity.
Feature-level fusion	Each sensor in the feature-level fusion system can collect feature data and extract feature data, and then, the fusion system extracts feature information from the sensor.
Decision-level fusion	First process the original data, identify, and extract the feature value, and get the result, and then, pass the result to the decision centre for fusion processing.

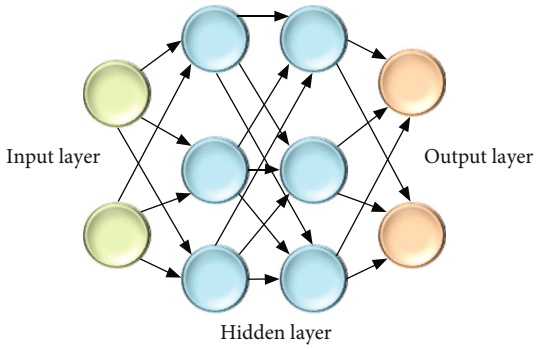

Figure 2: Schematic diagram of BPNN structure.

optimized, and the mean-square error (MSE) E is used as the loss function, as shown in

$$E = \frac{1}{2}(D - O)^2 = \frac{1}{2}\sum_{k=1}^{l}(d_k - o_k)^2. \tag{32}$$

D is the expected output value, O is the sample value of the output layer, and l is the sample number of the output layer.

The transfer function used by BPNN is the Sigmoid function, as shown in

$$f(x) = \frac{1}{1 + e^x}. \tag{33}$$

When the current is fed to the hth layer of the hidden layer, the kth training value can be expressed as

$$\text{net}_k^h = \sum_{j=1}^{m_k} y_j^h \bullet w_{j,k}^h. \tag{34}$$

Substituting Equations (33) and (34) into Equation (32), Equation (35) can be obtained:

$$E = \frac{1}{2}\sum_{k=1}^{l}\left(d_k - f\left(\text{net}_h^k\right)\right)^2 = \frac{1}{2}\sum_{k=1}^{l}\left[d_k - f\left(\sum_{j=1}^{m_k} y_j^h \bullet w_{j,k}^h\right)\right]^2. \tag{35}$$

When the current is fed to the first layer of the hidden layer, V_{ij} is the weight matrix of the first hidden layer and the input layer. From Equations (33) and (34), the jth training value of the first layer of the hidden layer is

$$\text{net}_j^1 = \sum_{i=1}^{n} x_i \bullet v_{i,j}. \tag{36}$$

Substituting Equation (36) into Equations (34) and (35), the error of the output layer can be expanded into

$$E = \frac{1}{2}\sum_{k=1}^{l}\left\{d_k - f\left[\sum_{j=1}^{m_h} w_{j,k}^h \bullet f\left(\sum_{i=1}^{n} x_i \bullet v_{i,j}\right)\right]\right\}^2. \tag{37}$$

The error of BPNN is a function of the weight value of each layer.

(3) The weight is adjusted. Taking Equation (37) as the objective function, it is necessary to adjust the weight matrix, in order to make the error E continue to decrease. To obtain the partial derivative of Equation (37), Equations (38) and (39) can be obtained:

$$\Delta w_{j,k_h}^h = -\eta\frac{\partial E}{\partial w_{j,k_h}^h}, \tag{38}$$

$$\Delta v_{i,j} = -\eta\frac{\partial E}{\partial v_{i,j}}. \tag{39}$$

η is the learning rate, and $\eta \in (0, 1)$. Then the weight value of the output layer can be adjusted to Equation (40) by the chain rule:

$$\begin{aligned}\Delta w_{j,k_h}^h &= -\eta\frac{\partial E}{\partial w_{j,k_h}^h} = \eta\left(-\frac{\partial E}{\partial \text{net}_{k_h}^h}\right)\frac{\partial \text{net}_{k_h}^h}{\partial w_{j,k_h}^h} \\ &= \eta\bullet\left(-\frac{\partial E}{\partial o_k}\right)\bullet\frac{\partial o_k}{\partial \text{net}_{k_h}^h}\bullet\frac{\partial \text{net}_{k_h}^h}{\partial w_{j,k_h}^h} \\ &= \eta\bullet(d_k - o_k)o_k(1 - o_k)\bullet y_k^h,\end{aligned} \tag{40}$$

where $k = 1, 2, \cdots, l$; $j = m_k$ is the number of neurons in the h th layer, and $k_h = 1$ is the number of samples in the output layer.

The specific algorithm flow of BPNN is shown in Figure 3.

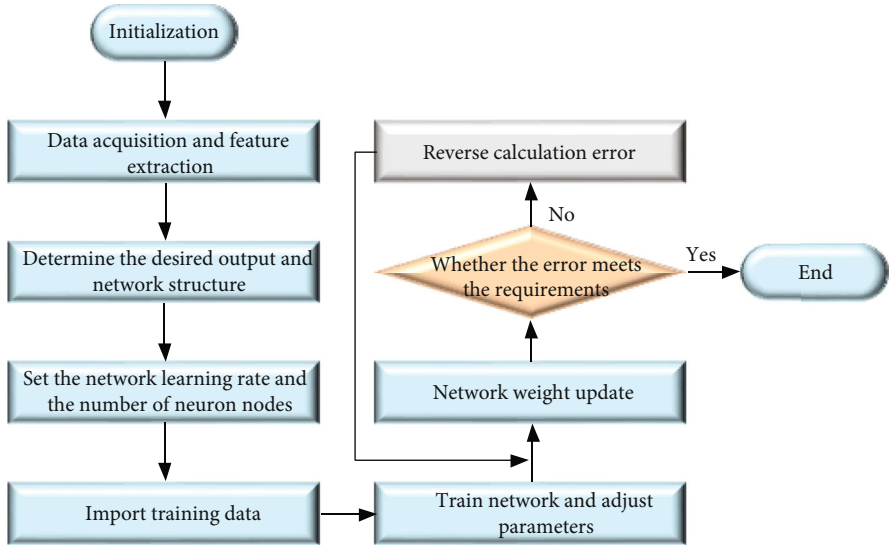

Figure 3: BPNN algorithm flow.

3.5. BPNN and Structural Damage Identification. The application of BPNN in structural damage identification is to match the actual detected structural features with the database of normal state features. The ability of pattern recognition is used to effectively and orderly classify measurement features. The learning and classification of BPNN is applied to data classification. The process of BPNN's identification of structural damage is divided into four steps:

Step 1: the structure of the neural network is built. The structure of the neural network selected is three layers The specific number of nodes in the hidden layer is determined by specific performance changes in network training and learning

Step 2: the sample data is processed. Commonly used methods to standardize data include dispersion standardization and standard deviation standardization. The standardization method used is the dispersion standardization method

Dispersion standardization: in fact, it is the method of maximum and minimum values. This method treats the data as

$$x = \frac{x_{ij} - \min x_{ij}}{\max x_{ij} - \min x_{ij}}, \quad i = 1, 2, \cdots, n, j = 1, 2, \cdots, m. \quad (41)$$

x represents the standardized data value, x_{ij} represents the unprocessed data value, min x_{ij} represents the minimum data value, and max x_{ij} represents the maximum data value.

Step 3: the network is trained. In the process of sample training, the parameters of the network are changed and adjusted in order to make the final output value consistent with the expected output value as much as possible

Step 4: the network is tested. The data of the test samples is used to perform a series of tests on the performance of those networks after the training is successful

3.6. Parameter Setting. The input vector used is composed of damage sensitive characteristics of reinforced concrete beams. Simple damage identification of structures is a binary classification problem, so the expected output is expressed as 0, 1. However, in the structural damage location, due to the need to distinguish different damage regions, the expected output is set in the form of vector.

The BPNN model is established on MATLAB, and the parameters are set through training and learning to construct the damage recognition model. According to the damage depth (20 mm, 5 mm) and the distance from the support (10 mm, 2500 mm), four groups are set for comparative analysis, A_1 (20 mm, 10 mm), A_2 (5 mm, 10 mm), and B_1 (20 mm, 2500 mm).

B_2 (5 mm, 2500 mm). The network training data and the test dataset are, respectively, set to 1×100 and 1×20 matrices. The network output structure is selected as a 1×20 matrix. The expected output is assigned a value. The label of the lossless dataset is recorded as 0, and the label of the damaged feature dataset is recorded as 1. The output result is close to 1 for lossless and close to 0 for damage. A total of 25 sets of data are randomly selected, of which 20 sets of data are training samples, and 5 sets are test samples.

4. Results and Discussion

4.1. Damage Identification Analysis by Single Feature. Use displacement mode data for network training and adjust parameters. The performance changes of the number of neurons in different hidden layers of the displacement mode are shown in Figure 4.

Figure 4 shows that for the displacement mode, as the number of neuron nodes increases, the MSE continues to decrease, and when the number of neuron nodes exceeds 7, it starts to increase again. Therefore, when the number of neurons in the hidden layer is 7 and the number of iterations is 200, the performance of the corresponding network is the best.

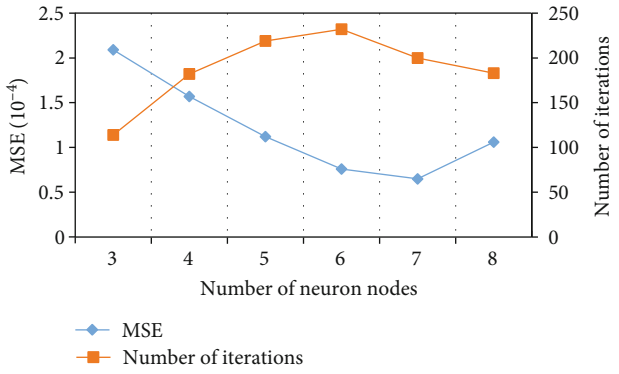

Figure 4: Performance changes of the number of neurons in different hidden layers in displacement mode.

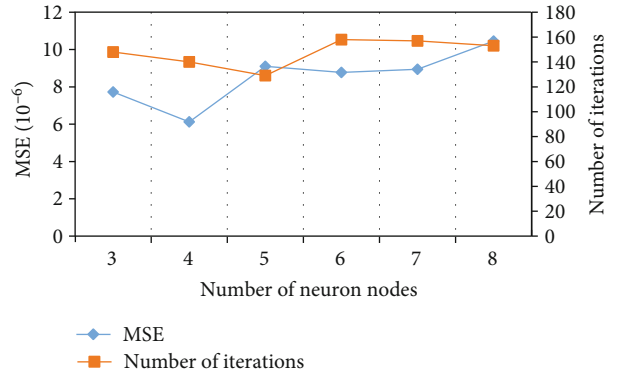

Figure 5: Performance changes of the number of neurons in different hidden layers with natural frequencies.

Use natural frequency data for network training and adjust parameters. The performance changes of the number of neurons in different hidden layers of natural frequencies are shown in Figure 5.

Figure 5 shows that for the natural frequency, when the number of neuron nodes exceeds 4, as the number of neuron nodes increases, the MSE continues to increase. When the number of neuron nodes is 4, the corresponding MSE value is the smallest. Therefore, when the number of neurons in the hidden layer is 4 and the number of iterations is 140, the performance of the corresponding network is the best.

Use MAC data for network training and adjust parameters. The performance changes of the number of neurons in different hidden layers of MAC are shown in Figure 6.

Figure 6 shows that for MAC, when the number of neuron nodes is 6, the corresponding MSE value is the smallest. Therefore, when the number of neurons in the hidden layer is 6, and the number of iterations is 195, the performance of the corresponding network is the best.

For different working conditions and feature sets, different data are tested. The output results are shown in Figures 7 and 8.

Figure 7 shows that when the damage centre is 10 mm away from the support, the damage depth is 20 mm, and the displacement mode is the characteristic data, the output values of the two sets of data numbered 3 and 4 are greater

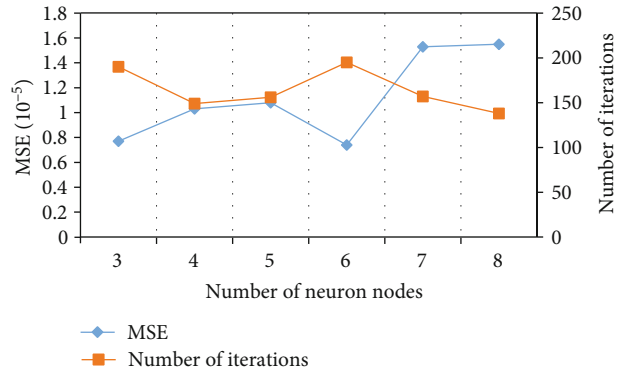

Figure 6: Performance changes of the number of neurons in different hidden layers of MAC.

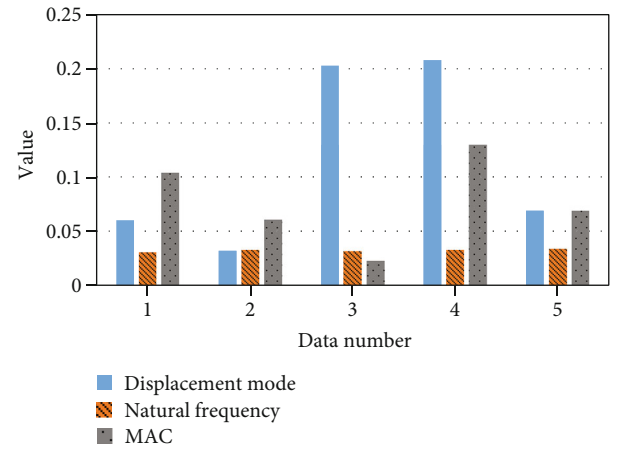

Figure 7: Structural damage identification results of A_1 (20 mm, 10 mm).

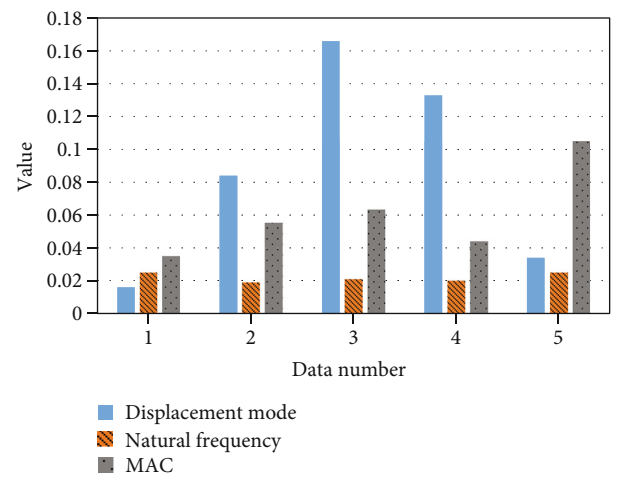

Figure 8: Structural damage identification results of B_1 (20 mm, 2500 mm).

than 0.2, so the expected output requirements are not met. When MAC and natural frequency are, respectively, characteristic data, the output values of the five sets of data all meet the requirements of expected output, and the expected damage identification is achieved. Figure 8 shows that when the

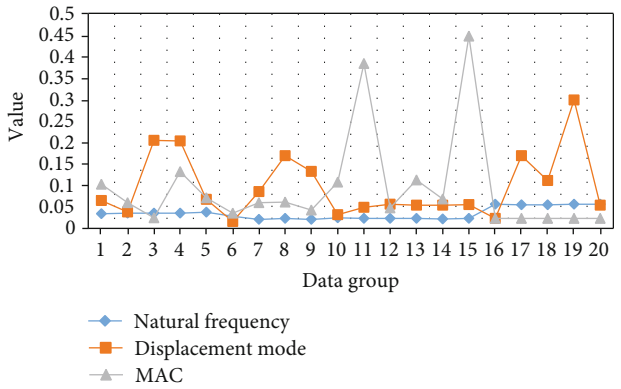

Figure 9: Difference between network output and expected output.

damage centre is 2500 mm away from the support and the damage depth is 20 mm, the output values of these three types of characteristic data are all less than 0.2. Therefore, they can meet the requirements of expected output and achieve the desired damage identification. In addition, the output result corresponding to the natural frequency has the best damage recognition effect in these three categories.

Compare the actual output value of the network with the expected value, and the absolute value of the difference between the two is shown in Figure 9.

Figure 9 shows that when the displacement mode is used as the characteristic data, the difference between the network output value and the expected value fluctuates relatively large, and the robustness is relatively poor. When the natural frequency is used as the sensitive feature of damage, the accuracy is the highest, the difference between the network output value and the expected value is the smallest, and the network output is the most stable. Therefore, its network recognition effect is also the best among these three categories.

4.2. Structural Damage Identification Analysis by Information Fusion. Five groups of data are extracted from the data of 10 mm and 2500 mm from the damage centre to the support, respectively, as test data, and the remaining data constituted the training set. 1 is the label of nondamaged data, and 0 is the label of damaged data. If the output value is greater than 0.85, it is close to 1. If the output value is less than 0.25, it is close to 0. When the damage depth is 20 mm, 5 mm, and the two depths are mixed, the node performance changes of the different hidden layer neurons corresponding to the network are shown in Figures 10–12.

Figure 10 shows that when the damage depth is 20 mm, and the number of neuron nodes is 7, the corresponding MSE value is the smallest. Therefore, when the number of neurons in the hidden layer is 7 and the number of iterations is 205, the performance of the corresponding network is the best.

Figure 11 shows that when the damage depth is 5 mm, the MSE fluctuates up and down as the number of neuron nodes increases. When the number of neuron nodes is 5, the corresponding MSE value is the smallest. Therefore, when the number of neurons in the hidden layer is 5 and

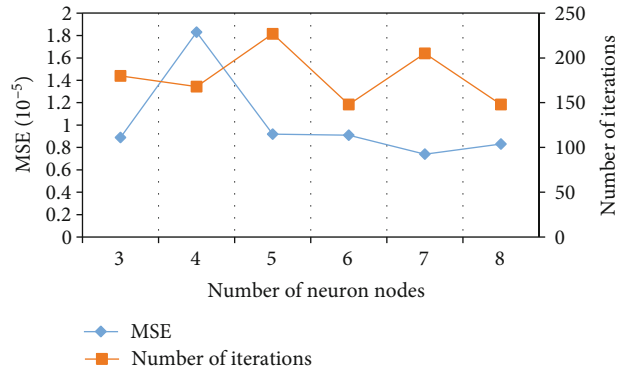

Figure 10: Performance changes in the number of neurons in different hidden layers with a damage depth of 20 mm.

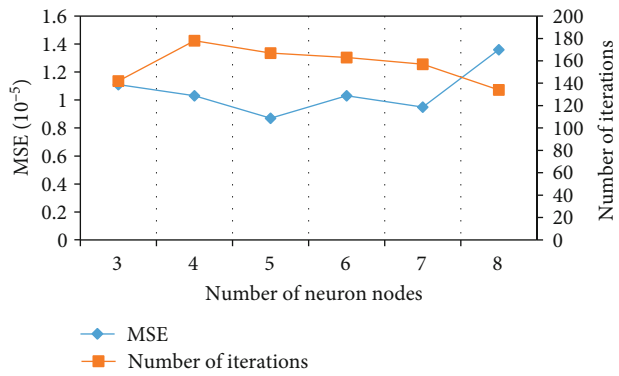

Figure 11: Performance changes of the number of neurons in different hidden layers with a damage depth of 5 mm.

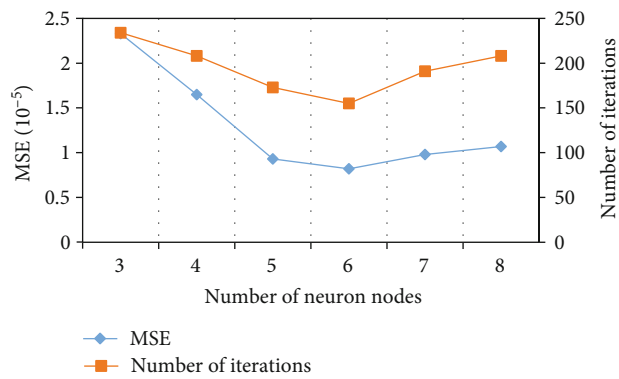

Figure 12: Performance changes of the number of neurons in different hidden layers with different damage sizes.

the number of iterations is 167, the performance of the corresponding network is the best.

Figure 12 shows that when the feature data with damage depths of 20 mm and 5 mm together form the data of the network training set, the MSE decreases and then increases with the increase of the number of neuron nodes. When the number of neuron nodes is 6, the corresponding MSE value is the smallest. Therefore, when the number of neurons in the hidden layer is 6 and the number of iterations is 155, the performance of the corresponding network is the best.

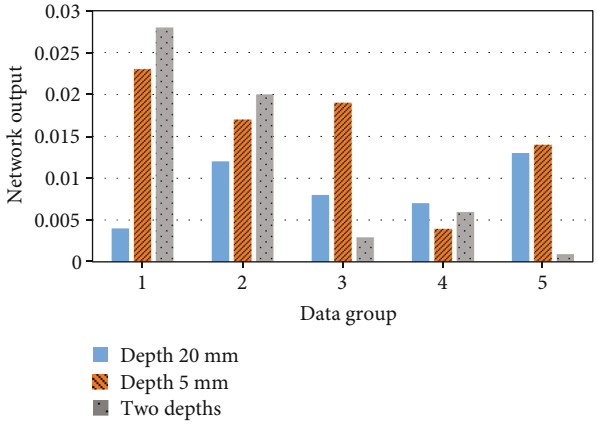

Figure 13: Data fusion damage identification result of 10 mm distance from the damage centre to the support.

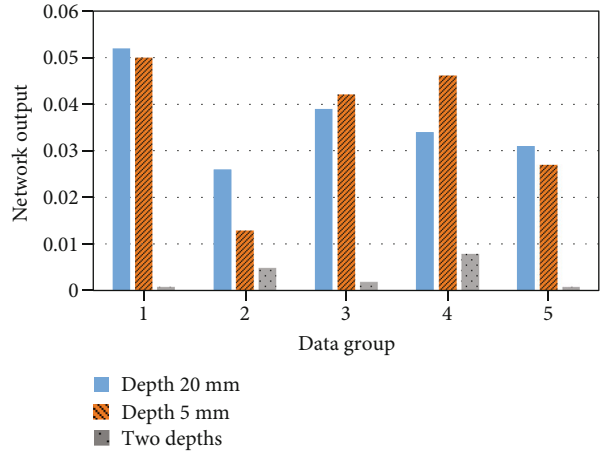

Figure 14: Damage identification result of data fusion of 2500 mm from the damage centre to the support.

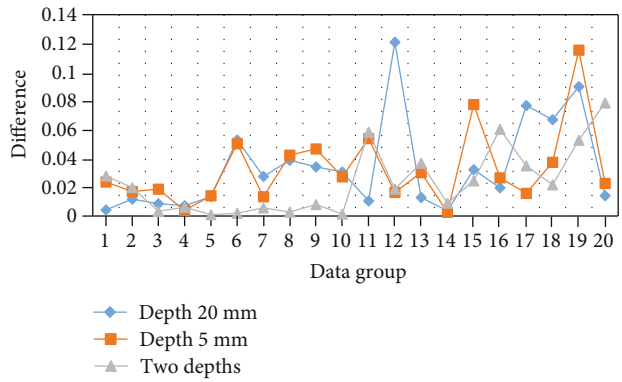

Figure 15: The difference between the output of the structural damage identification network by information fusion and the expected output.

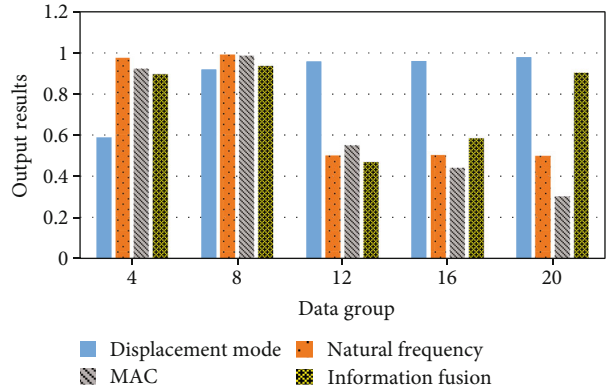

Figure 16: Output result of damage location.

In these three different training situations, the actual output values of the network are compared, and the result analysis is shown in Figure 13. The actual output value of the network with the expected value are compared, and the difference between the two is shown in Figure 14.

Figure 13 shows that the distance from the damage centre to the support is 10 mm, and the data of the network training set consists of a damage depth of 20 mm and a damage depth of 5 mm; the corresponding output values are all less than 0.2. Therefore, it can meet the requirements of expected output and achieve the desired damage identification.

Figure 14 shows that when the distance from the damage centre to the support is 2500 mm, and the data of the network training set consists of a damage depth of 20 mm and a damage depth of 5 mm; the corresponding output values are all less than 0.2. Therefore, they can meet the requirements of expected output and achieve the desired damage identification. When the feature data with damage depths of 20 mm and 5 mm together form the data of the network training set, the corresponding output result is closer to the expected value, so the damage recognition effect is the best in these three categories.

Figure 15 shows that comparing the output of the network with a mixture of two damage depths with the output of a single damage depth, when the feature data with damage depths of 20 mm and 5 mm together form the data of the network training set, the corresponding accuracy is higher.

4.3. Damage Location Analysis. Structural damage identification can not only determine whether the structure is in a safe state but also provide a more accurate basis for the safety identification of the structure by identifying the location of the structural damage, which is easy to maintain and inspect the structure. The output result of damage location is shown in Figure 16.

Figure 16 shows that the accuracy of damage location by the displacement mode structure is relatively high. Compared with the accuracy of single damage location by natural frequency and MAC, the accuracy of damage recognition by information fusion will be higher. This shows that the application of information fusion technology in damage location is still feasible.

By the above discussion, in the current neural network model, the displacement mode can realize the damage location when it is used as the characteristic parameter. But the network error is larger than that when it is used for damage

identification. For the damage of other characteristic parameters on certain locations, it is impossible to locate the damage. The possible influencing factors include:

(1) Compared with damage identification, damage location requires more accurate analysis of feature data. When BPNN performs operations with higher accuracy requirements, it also requires higher data requirements and requires more complete datasets to complete the learning of structural characteristics

(2) The selected feature data are theoretically sensitive to damage location, but different features have different sensitivities to damage location. As the whole characteristic of structure, natural frequency is affected by other factors besides damage location, so there is a big error in reflecting damage location. The displacement mode is more sensitive to the structural damage location, so the recognition accuracy is relatively high. The MAC values obtained from the vibration mode parameters are also more sensitive to the damage and less sensitive to the damage location

5. Conclusions

Nowadays, with the continuous development of science and technology, AI is used in the damage identification of structures, which helps to improve the calculation speed of the system. As a result, the accuracy of structural damage detection is improved. The damage recognition of the building structure is studied, BPNN and information fusion are used as the basis, and the BPNN is established and trained. The displacement mode, natural frequency, MAC, and three kinds of information fusion with only one characteristic information are used as input data, and the result of BPNN identification damage is analysed. The results show that when the natural frequency is used as the sensitive feature of damage, the accuracy is the highest, the difference between the network output value and the expected value is the smallest, and the network output is the most stable. Therefore, its network recognition effect is also the best among these three categories. Comparing the output of the mixed network of two damage depths with the output of a single damage depth, it corresponds to higher accuracy and more accurate damage identification. The research provides a reference for the optimization of building survey technology and has certain practical value. The disadvantage is that when selecting the structural parameters, the influence of some external factors such as the environment or the instrument is not considered. So, in the future, it is necessary to establish a system that can be used in a complex environment.

Data Availability

The key source code and data used to support the findings of this paper are available upon request to the corresponding author.

Conflicts of Interest

The authors declare that there are no conflicts of interest regarding the publication of this paper.

References

[1] C. Zhou, J. G. Chase, G. W. Rodgers, and C. Iihoshi, "Damage assessment by stiffness identification for a full-scale three-story steel moment resisting frame building subjected to a sequence of earthquake excitations," *Bulletin of Earthquake Engineering*, vol. 15, no. 12, pp. 5393–5412, 2017.

[2] V. Ryabtsev and V. Vengrinovich, "Damage identification using the moving fractal method for automated monitoring," *Construction of Unique Buildings and Structures*, vol. 68, no. 5, pp. 52–61, 2018.

[3] Z. Ding, J. Li, and H. Hao, "Structural damage identification by sparse deep belief network using uncertain and limited data," *Structural Control and Health Monitoring*, vol. 27, no. 5, article e2522, 2020.

[4] X. Tang, Q. Zhang, and J. Wu, "Damage identification and early warning for a single-layer cable net building by structural health monitoring," in *Proceedings of IASS Annual Symposia, International Association for Shell and Spatial Structures (IASS)*, pp. 1–8, Boston, USA, 2018.

[5] M. Gordan, H. A. Razak, Z. Ismail, and K. Ghaedi, "Recent developments in damage identification of structures using data mining," *Latin American Journal of Solids and Structures*, vol. 14, no. 13, pp. 2373–2401, 2017.

[6] C. Liu, H. Sui, and L. Huang, "Identification of building damage from UAV-based photogrammetric point clouds using supervoxel segmentation and latent Dirichlet allocation model," *Sensors*, vol. 20, no. 22, p. 6499, 2020.

[7] C. Zhou, J. G. Chase, and G. W. Rodgers, "Efficient hysteresis loop analysis-based damage identification of a reinforced concrete frame structure over multiple events," *Journal of Civil Structural Health Monitoring*, vol. 7, no. 4, pp. 541–556, 2017.

[8] M. Huang, Y. Lei, and X. Li, "Structural damage identification based on l1regularization and bare bones particle swarm optimization with double jump strategy," *Mathematical Problems in Engineering*, vol. 2019, Article ID 5954104, 16 pages, 2019.

[9] Y. Yu, C. Wang, X. Gu, and J. Li, "A novel deep learning-based method for damage identification of smart building structures," *Structural Health Monitoring*, vol. 18, no. 1, pp. 143–163, 2019.

[10] J. Liu, Z. Lu, and M. Yu, "Damage identification of nonclassically damped shear building by sensitivity analysis of complex modal parameter," *Journal of Sound and Vibration*, vol. 438, pp. 457–475, 2019.

[11] X. Wang, X. Zhang, and M. M. Shahzad, "A novel structural damage identification scheme based on deep learning framework," *Structure*, vol. 29, pp. 1537–1549, 2021.

[12] Y. Gao and K. M. Mosalam, "Deep transfer learning for image-based structural damage recognition," *Computer-Aided Civil and Infrastructure Engineering*, vol. 33, no. 9, pp. 748–768, 2018.

[13] M. Lopez-Pacheco, J. Morales-Valdez, and W. Yu, "Frequency domain CNN and dissipated energy approach for damage detection in building structures," *Soft Computing*, vol. 24, no. 20, pp. 15821–15840, 2020.

[14] C. Liu, C. Liu, C. Liu, X. Huang, J. Miao, and W. Xu, "Fire damage identification in RC beams based on support vector machines considering vibration test," *KSCE Journal of Civil Engineering*, vol. 23, no. 10, pp. 4407–4416, 2019.

[15] X. Xu, Q. Wang, D. Niu, and L. Zhang, "Synergistic effect evaluation of main and auxiliary industry of power grid based on the information fusion technology from the perspective of

sustainable development of enterprises," *Sustainability*, vol. 10, no. 2, p. 457, 2018.

[16] Q. Tan, P. Wang, J. Hu, P. Zhou, M. Bai, and J. Hu, "The application of multi-sensor target tracking and fusion technology to the comprehensive early warning information extraction of landslide multi-point monitoring data," *Measurement*, vol. 166, article 108044, 2020.

[17] P. Zhang, T. Li, G. Wang et al., "Multi-source information fusion based on rough set theory: a review," *Information Fusion*, vol. 68, pp. 85–117, 2021.

[18] L. Liu, Z. Zuo, Y. Wang, and F. R. Xu, "A fast multi-source information fusion strategy based on FTIR spectroscopy for geographical authentication of wild *Gentiana rigescens*," *Microchemical Journal*, vol. 159, article 105360, 2020.

[19] Y. Xu, Y. Wu, H. Gao, S. Song, Y. Yin, and X. Xiao, "Collaborative APIs recommendation for artificial intelligence of things with information fusion," *Future Generation Computer Systems*, vol. 125, pp. 471–479, 2021.

[20] K. Gong, D. D. He, S. Y. Chen, S. W. Jing, and Y. L. Zheng, "BP neural network analysis for identification of explosive in package by tagged neutron method," *Nuclear Instruments and Methods in Physics Research Section A: Accelerators, Spectrometers, Detectors and Associated Equipment*, vol. 1017, article 165810, 2021.

[21] Z. Wang, B. Wang, C. Liu, and W. S. Wang, "Improved BP neural network algorithm to wind power forecast," *The Journal of Engineering*, vol. 2017, no. 13, pp. 940–943, 2017.

[22] K. Cui and X. Jing, "Research on prediction model of geotechnical parameters based on BP neural network," *Neural Computing and Applications*, vol. 31, no. 12, pp. 8205–8215, 2019.

[23] A. Yang, Y. Zhuansun, C. Liu, J. Li, and C. Zhang, "Design of intrusion detection system for internet of things based on improved BP neural network," *IEEE Access*, vol. 7, pp. 106043–106052, 2019.

[24] J. Li, D. Zhao, B. F. Ge, K. W. Yang, and Y. W. Chen, "A link prediction method for heterogeneous networks based on BP neural network," *Physica A: Statistical Mechanics and its Applications*, vol. 495, pp. 1–17, 2018.

[25] D. J. Li, Y. Y. Li, J. X. Li, and Y. Fu, "Gesture recognition based on BP neural network improved by chaotic genetic algorithm," *International Journal of Automation and Computing*, vol. 15, no. 3, pp. 267–276, 2018.

[26] J. Lyu and J. Zhang, "BP neural network prediction model for suicide attempt among Chinese rural residents," *Journal of Affective Disorders*, vol. 246, pp. 465–473, 2019.